

Chapter 8

COARSENING

In the previous chapter, we discussed the coarsening of kinetic Ising models starting from an initial homogeneous high-temperature phase and suddenly lowering the temperature (quenching) below the critical temperature. The ensuing coarsening is complex (see Fig. 7.6), and considerable effort has been devoted to developing simpler continuum descriptions. While we lose a direct connection to individual spins in such a formulation, continuum theories, while still quite formidable, are typically simpler than their discrete counterparts. We will investigate some of the simplest geometries for coarsening dynamics that can be solved explicitly. This includes freely diffusing interfaces in the absence of interactions, the single domain wall, and a droplet of one phase that is immersed into another phase. For such cases, many aspects of the evolution can be found analytically. For the more generic case of a random initial condition, the continuum approach provides many new insights that seem to be impossible to obtain by a description at the level of individual spins.

8.1 The Models

We tacitly assume that the order parameter is a scalar, and will state otherwise explicitly. We generally have in mind magnetic systems and will use the terminology associated with such systems. However, this usage is more reflective of tradition rather than the dominant application of coarsening. Even for the simplest case of systems with a scalar order parameter, the distinction between non-conservative and conservative dynamics is crucially important, and we now outline the generic models of these two dynamics.

Non-conservative dynamics

The basic ingredients that underlie non-conservative Landau-Ginzburg dynamics are the following:

- We deal with a continuous coarse-grained order parameter, or magnetization, $m(\mathbf{x}, t)$ rather than a binary Ising variable $\sigma = \pm 1$ by defining $m(\mathbf{x}, t) \equiv \ell^{-d} \sum \sigma$. That is, $m(\mathbf{x}, t)$ is the average magnetization in a block of linear dimension ℓ ; the sum runs over the ℓ^d spins in the block centered at \mathbf{x} . Here ℓ should be much greater than the lattice spacing a and much smaller than the system size \mathcal{L} . These restrictions give a coarse-grained magnetization that varies smoothly on a scale greater than ℓ that can accommodate a non-trivial spatial dependence. This coarse-graining is appropriate over the time range where the typical domain size is much larger than ℓ and much smaller than \mathcal{L} .
- We describe the thermodynamics of the system by the coarse-grained Landau free-energy functional

$$F[m(\mathbf{x})] = \int \left[\frac{1}{2} |\nabla m(\mathbf{x})|^2 + V(m(\mathbf{x})) \right] d\mathbf{x}, \quad (8.1)$$

where the potential $V(m)$ has a double-well structure with minima corresponding to the equilibrium states. The standard example is $V(m) = \frac{1}{2}(1 - m^2)^2$ for systems with two degenerate minima; we always assume that the minima occur at $m = \pm 1$ and that $V(\pm 1) = 0$. While this coarse-grained

free energy is intuitively plausible — it combines the Landau mean-field theory with the lowest order contribution due to spatial variation of the order parameter — it is not possible to derive Eq. (8.1) from first principles starting with a microscopic model, such as the Ising model.

- The final step in constructing a coarse-grained dynamical description is also phenomenological: we simply assert that the order parameter changes at a rate that is proportional to the local thermodynamic force $\frac{\delta F}{\delta m(\mathbf{x},t)}$, where $\frac{\delta}{\delta m(\mathbf{x},t)}$ denotes the functional derivative with respect to m at position \mathbf{x} . Thus we are considering *overdamped* dynamics because there is no second time derivative in the equation of motion. This assumption is equivalent to ignoring inertia. Absorbing a coefficient of proportionality into the time scale, we thus arrive at the *time-dependent Ginzburg-Landau (TDGL) equation*

$$\frac{\partial m}{\partial t} = -\frac{\delta F}{\delta m} = \nabla^2 m - V'(m). \quad (8.2)$$

The TDGL equation is one of the central equations of coarsening.

There are three important aspects of the TDGL equation that merit emphasis. First, even though the TDGL equation is widely accepted and used, this dynamics is impossible to derive from a microscopic theory, such as the Ising-Glauber model. Second the TDGL equation is purely dissipative. This feature can be easily shown by computing the change in the free energy as a function of time:

$$\frac{dF}{dt} = \int \frac{\delta F}{\delta m} \frac{\partial m}{\partial t} d\mathbf{x} = - \int \left(\frac{\delta F}{\delta m} \right)^2 \mu d\mathbf{x} \leq 0.$$

Thus a system governed by the TDGL equation simply “flows” down the free energy gradient until one of the two potential minima is reached. A third important point is that the TDGL equation has a natural interpretation as a reaction-diffusion process. For the standard potential $V(m) = \frac{1}{2}(1 - m^2)^2$, the explicit TDGL equation is:

$$\frac{\partial m}{\partial t} = \nabla^2 m + 2m(1 - m^2). \quad (8.3)$$

If we view m as a density, then the above equation describes the evolution of a diffusing population of particles that give birth, $m \rightarrow 2m$, and undergo 3-body coalescence, $3m \rightarrow m$. The rate equation for this reaction, $\frac{dm}{dt} = 2m - 2m^3$, has an unstable fixed point at $m = 0$ and a stable fixed point at $m = 1$. When diffusion is included, the resulting equation of motion (8.3) describes the infiltration of a stable high-density phase ($m = 1$) into a low-density ($m = 0$) region. In fact, Eq. (8.3) is just one example of the family of self-regulating reactions of the form

$$\frac{\partial m}{\partial t} = \nabla^2 m + f(m), \quad (8.4)$$

with $f(0) = f(1) = 0$, $f(m) > 0$ for $0 < m < 1$, and $f(m)$ having a single maximum in the range $[0, 1]$. The most famous of this class of equations arises when $f(m) = m(1 - m)$, and is known as the Fisher-Kolmogorov-Petrovsky-Piscounov (FKPP) equation (see the highlight below).

The FKPP Equation

The FKPP equation

$$\frac{\partial A}{\partial t} = D\nabla^2 A + kA(N - A), \quad (8.5)$$

describes the evolution of a diffusing population where individuals give birth ($A \rightarrow A + A$) and quadratically self-regulate ($A + A \rightarrow A$). If spatial fluctuations are neglected, then in the resulting rate equation, $\dot{A} = A(N - A)$, there is a stable fixed point when $A = N$ and an unstable fixed point for $A = 0$. Here N should be viewed as the maximum number of particles that can be accommodated on a single site in the lattice version of the reaction. Starting with any non-zero density in a finite system, a final density of N is reached. An important example for population biology is the case where $A = N$ in the half-space $x < 0$ and $A = 0$ for $x > 0$. By diffusion alone, the sharp interface between these two regions would become smoother. However, because of the interplay between diffusion and reaction, the stable high-density phase propagates as a stationary wave into the low-density phase.

Let's study the basics of this wave propagation in one dimension. Proceeding in a naive way, we assume that the stable state infiltrates as a stationary propagating wave. As a preliminary, it is useful to rescale the density by $A \rightarrow A/N$, time by $t \rightarrow kt$, and then the length by $x \rightarrow x\sqrt{k/D}$ to non-dimensionalize the FKPP equation to $\frac{\partial A}{\partial t} = \nabla^2 A + A(1 - A)$. The simplest assumption is that the leading edge of this wave decays exponentially with position:

$$A(x, t) \sim e^{-\lambda(x-vt)}.$$

Substituting this form into Eq. (8.5) and dropping the non-linear term that is negligible at the leading edge of the wave, we obtain the dispersion relation

$$v = \lambda + \frac{1}{\lambda}.$$

Thus the velocity ostensibly depends on λ and we can only surmise that $v \geq 2$. The equation of motion does not provide any information about which velocity is selected. Nature appears to be wise, however, and typically “selects” the minimum velocity $v_{\min} = 2$ that arises when $\lambda = 1$. In fact, for most “reasonable” initial conditions, this minimum velocity is the one that is actually selected.

More precisely, if the initial density decays as $e^{-\lambda_0 x}$ with $\lambda_0 > 1$, then the leading edge of the wave asymptotically evolves to an exponential with decay parameter $\lambda = 1$ and velocity $v = v_{\min}$. We call such wavefronts “sharp”. On the other hand, if $\lambda_0 < 1$, then the leading edge of the wave preserves this slower decay, $e^{-\lambda_0(x-vt)}$, and the velocity is $v = \lambda_0 + \lambda_0^{-1} > v_{\min}$. However, this behavior is still not the full story! A more complete analysis for the FKPP equation shows that for an initially sharp wavefront the velocity slowly approaches its asymptotic value as $v(t) = v_{\min}(1 - 3/Nt)$. Moreover, in the leading edge of the wave, the density is small and there is no reason that the evolution of the first few invaders can even be described by a continuum equation. If one accounts for the discrete nature of the particles, then the wave velocity is reduced compared to the continuum value: $v = v_{\min}(1 - \pi^2/\ln^2 N)$ — surprisingly rich behavior from such a basic equation of motion.

Conservative dynamics

In two-component alloy systems, the natural order parameter is the difference in the concentration of the two constituent elements. By its construction, this order parameter is conserved in an isolated piece of alloy. Thus dynamics different from the TDGL is needed to account for this microscopic conservation of material. At a phenomenological level, we seek a governing dynamical equation that ensures that the flux of atoms of each element of the alloy can be expressed in the form of a (conserved) continuity equation

$$\frac{\partial m}{\partial t} + \nabla \cdot \mathbf{J} = 0, \quad (8.6)$$

where we again consider overdamped dynamics so that the equation of motion is first order in time. In Eq. (8.6), the flux vector \mathbf{J} should depend on the order parameter through the free energy (8.1). The

simplest choice that is both conservative and involves simple gradient flow is $\mathbf{J} \propto -\nabla \frac{\delta F}{\delta m}$. We again absorb the proportionality factor into the time scale to then obtain the equation of motion

$$\frac{\partial m}{\partial t} = \nabla^2 \frac{\delta F}{\delta m} = -\nabla^2 [\nabla^2 m - V'(m)]. \quad (8.7)$$

This is the *Cahn-Hilliard (CH) equation* for zero-temperature conservative dynamics.

The absence of thermal noise in Eqs. (8.2) & (8.7) suggests that we are effectively dealing with systems at zero temperature. To phenomenologically model the behavior at a positive temperature, we should add a (Langevin) noise term to the right-hand side of (8.2) or (8.7). There is a belief that this additional term should not change qualitative dynamical behavior as long as the temperature is below the critical temperature T_c . This belief boils down to the hypothesis that under renormalization, there are three possible behaviors:

- zero-temperature dynamics in which dynamical behavior is essentially the same for all $T < T_c$;
- critical dynamics ($T = T_c$);
- infinite-temperature dynamics in which the dynamical behavior for all $T > T_c$ are essentially the same, and trivial.

In this chapter, we will discuss zero-temperature dynamics because this case embodies many of the outstanding issues associated with coarsening. Typically, one starts with the initial temperature $T_i = \infty$ where the system is completely disordered and quenches the system to $T_f = 0$. The coarse-grained form of this disordered initial condition is

$$\langle m(\mathbf{x}, 0) \rangle = 0, \quad \langle m(\mathbf{x}, 0) m(\mathbf{x}', 0) \rangle = \delta(\mathbf{x} - \mathbf{x}'). \quad (8.8)$$

Thus the mathematical challenge is to determine the long-time behavior of the solutions of the *deterministic* nonlinear partial differential equations (8.2) and (8.7) subject to the *random* initial conditions (8.8).

8.2 Free Evolution

Numerical and analytical work has clearly shown that the solutions of (8.2) and (8.7) exhibit scaling, *i.e.*, a scale-invariant coarsening domain mosaic morphology develops at late times. This morphology is (statistically) independent of time when all lengths are rescaled by the typical domain size $L(t)$. This length scale grows algebraically with time, $L(t) \sim t^z$, with a nearly universal dynamical exponent z :

$$z = \begin{cases} 1/2 & \text{(TDGL);} \\ 1/3 & \text{(CH);} \end{cases} \quad (8.9)$$

for systems with a scalar order parameter. One important exception to Eq. (8.9) is one dimension, where we shall derive that domains grow logarithmically in time for the TDGL equation, $L(t) \sim \ln t$, so that the dynamical exponent $z = 0$.

As always, scaling greatly simplifies the description of the dynamics. The evidence in favor of scaling is compelling, but it has not been proven except for the TDGL in one dimension and for a small class of microscopic models, such as the one-dimensional Ising-Glauber model and the n -vector model with $n = \infty$. It is therefore important to show that scaling arises in the TDGL and the CH equations, even for an oversimplified setting. Such an example is provided by the toy model where the potential vanishes, $V(m) = 0$. The dynamical equation then reduces to the diffusion equation, $\frac{\partial m}{\partial t} = \nabla^2 m$, for a non-conserved order parameter, and to the bidiffusion equation, $\frac{\partial m}{\partial t} = -\nabla^4 m$, for a conserved order parameter. In these cases, the presence of a single growing length scale, $L(t) \sim t^{1/2}$ (TDGL), and $L(t) \sim t^{1/4}$ (CH), is obvious from dimensional analysis (see the subsections on dimensional analysis and scaling in Sec. 1.1 for further discussion of this point).

If a spin system is initially in the random state specified by Eq. (8.8), then the magnetization remains zero throughout the evolution. We therefore need two-body correlation functions to investigate the nature of

the coarsening; we already encountered this same issue in our study of the voter model and the Ising-Glauber model in the previous chapter. We thus define the two-body correlation function

$$C(\mathbf{r}_1, t_1, \mathbf{r}_2, t_2) \equiv \frac{\langle m(\mathbf{r}_1, t_1) m(\mathbf{r}_2, t_2) \rangle}{\sqrt{\langle m^2(\mathbf{r}_1, t_1) \rangle \langle m^2(\mathbf{r}_2, t_2) \rangle}} \quad (8.10)$$

to probe the domain structure at two different space-time points. Our choice for the normalization makes the correlation function dimensionless. For simplicity, we use the shorthand $1 \equiv (\mathbf{x}_1, t_1)$ and $2 \equiv (\mathbf{x}_2, t_2)$. Translational invariance implies that $C(1, 2) = C(\mathbf{r}, t_1, t_2)$ with $\mathbf{r} = \mathbf{r}_1 - \mathbf{r}_2$. It is also useful to explicitly study the *autocorrelation function* $A(t_1, t_2) = C(\mathbf{0}, t_1, t_2)$ that measures the probability that the sign of the magnetization coincides at times t_1 and t_2 .

Let's begin by investigating coarsening in the potential-free TDGL (diffusion) equation

$$\frac{\partial m}{\partial t} = \nabla^2 m \quad (8.11)$$

for the random initial condition of Eq. (8.8). The solution is

$$m(\mathbf{r}_1, t) = \frac{1}{(4\pi t)^{d/2}} \int m(\mathbf{z}_1, 0) e^{-(\mathbf{r}_1 - \mathbf{z}_1)^2/4t} d\mathbf{z}_1.$$

Then the average of the product of the magnetization at two different space-time points is

$$\begin{aligned} \langle m(\mathbf{r}_1, t_1) m(\mathbf{r}_2, t_2) \rangle &= \frac{1}{[(4\pi)^2 t_1 t_2]^{d/2}} \iint \underbrace{\langle m(\mathbf{z}_1, 0) m(\mathbf{z}_2, 0) \rangle}_{\delta(\mathbf{z}_1 - \mathbf{z}_2)} e^{-(\mathbf{r}_1 - \mathbf{z}_1)^2/4t_1} e^{-(\mathbf{r}_2 - \mathbf{z}_2)^2/4t_2} d\mathbf{z}_1 d\mathbf{z}_2 \\ &= \frac{1}{[(4\pi)^2 t_1 t_2]^{d/2}} \int e^{-(\mathbf{r}_1 - \mathbf{z})^2/4t_1} e^{-(\mathbf{r}_2 - \mathbf{z})^2/4t_2} d\mathbf{z} \\ &= \frac{1}{[(4\pi)^2 t_1 t_2]^{d/2}} \int e^{-\mathbf{r}_1^2/4t_1} e^{-\mathbf{r}_2^2/4t_2} e^{-z^2(1/4t_1 + 1/4t_2)} e^{\mathbf{z} \cdot (\mathbf{r}_1/2t_1 + \mathbf{r}_2/2t_2)} . \end{aligned}$$

We perform the integral in the last line by completing the square in the exponential to give

$$\langle m(\mathbf{r}_1, t_1) m(\mathbf{r}_2, t_2) \rangle = \frac{1}{[4\pi(t_1 + t_2)]^{d/2}} e^{-(\mathbf{r}_1 - \mathbf{r}_2)^2/4(t_1 + t_2)} . \quad (8.12)$$

Finally, the normalized two-body correlation function defined by Eq. (8.10) is

$$C(1, 2) = \left[\frac{2\sqrt{t_1 t_2}}{t_1 + t_2} \right]^{d/4} e^{-(\mathbf{r}_1 - \mathbf{r}_2)^2/4(t_1 + t_2)} . \quad (8.13)$$

Let's now study coarsening for the potential-free CH (bidiffusion) equation

$$\frac{\partial m}{\partial t} = -\nabla^4 m . \quad (8.14)$$

Notice that the right-hand side now has a minus sign. The simplest way to solve the bidiffusion (and the diffusion) equations is with Fourier transforms. Using the Fourier expansion $m(\mathbf{r}, t) = (2\pi)^{-d} \int \hat{m}(\mathbf{k}, t) e^{-i\mathbf{k} \cdot \mathbf{r}} d\mathbf{k}$ reduces (8.14) to an algebraic equation whose solution is simply $\hat{m}(\mathbf{k}, t) = \hat{m}_0(\mathbf{k}) e^{-k^4 t}$, with $\hat{m}_0(\mathbf{k}) \equiv \hat{m}(\mathbf{k}, t = 0)$. Inverting this Fourier transform gives

$$m(\mathbf{x}, t) = (2\pi)^{-d} \int \hat{m}_0(\mathbf{k}) e^{-i\mathbf{k} \cdot \mathbf{x} - k^4 t} d\mathbf{k}. \quad (8.15)$$

For the white noise initial condition, the initial value of the correlation function in Fourier space is just

$$\langle \hat{m}_0(\mathbf{k}) \rangle = 0, \quad \langle \hat{m}_0(\mathbf{k}) \hat{m}_0(\mathbf{k}') \rangle = (2\pi)^d \delta(\mathbf{k} + \mathbf{k}'). \quad (8.16)$$

Using these facts, the mean-square magnetization $\langle m^2(\mathbf{x}, t) \rangle$ can be immediately found from Eqs. (8.8), (8.15), & (8.16), and the result is:

$$\langle m^2(\mathbf{x}, t) \rangle = (2\pi)^{-d} \int e^{-2k^4 t} d\mathbf{k} = B_d (2t)^{-d/4}, \quad (8.17)$$

where $B_d = (2\pi)^{-d} \Omega_d \Gamma(d/4)/4$, $\Omega_d = 2\pi^{d/2}/\Gamma(d/2)$ is the area of the unit sphere in d dimensions, Γ is the Euler gamma function, and the subscript d refers to the spatial dimension of the system.

Similarly, the correlation function is

$$\langle m(1) m(2) \rangle = (2\pi)^{-d} \int e^{-i\mathbf{k} \cdot \mathbf{r} - k^4(t_1+t_2)} d\mathbf{k}. \quad (8.18)$$

When spatial points coincide, $\mathbf{r} = \mathbf{0}$, we obtain the autocorrelation function

$$A(t_1, t_2) = \left[\frac{2\sqrt{t_1 t_2}}{t_1 + t_2} \right]^{d/4}, \quad (8.19)$$

which has the same form for both the diffusion [Eq. (8.13)] and the bidiffusion equation. If the spatial points are different, $\mathbf{r}_1 \neq \mathbf{r}_2$, we perform the integral in Eq. (8.18) by introducing spherical coordinates in \mathbf{k} -space for $d \geq 2$ so that $\mathbf{k} \cdot \mathbf{r} = kr \cos \theta$ and $d\mathbf{k} = k^{d-1} \Omega_{d-1} \sin^{d-2} \theta d\theta dk$ to give

$$\langle m(1) m(2) \rangle = \frac{\Omega_{d-1}}{(2\pi)^d} \int_0^\infty k^{d-1} e^{-k^4(t_1+t_2)} F_d(kr) dk,$$

where

$$F_d(u) = \int_0^\pi (\sin \theta)^{d-2} e^{-iu \cos \theta} d\theta.$$

This integral may be readily determined for $d \leq 3$ and the two-body correlation function $C(r, t_1, t_2)$ is:

$$C(r, t_1, t_2) = \begin{cases} \frac{2(4t_1 t_2)^{1/8}}{\Gamma(1/4) r} \int_{-\infty}^\infty \cos q e^{-q^4 \tau} dq & d = 1; \\ \frac{4(4t_1 t_2)^{1/4}}{\sqrt{\pi} r^2} \int_0^\infty q I_0(q) e^{-q^4 \tau} dq & d = 2; \\ \frac{2(4t_1 t_2)^{3/8}}{\Gamma(3/4) r^3} \int_0^\infty q \sin q e^{-q^4 \tau} dq & d = 3. \end{cases} \quad (8.20)$$

In these equations, we use shorthand notations $q = kr$, $\tau = (t_1 + t_2)/r^4$, and I_0 is the modified Bessel function of order 0.

Finally, the *temporally normalized* correlation function $G(\mathbf{r}, t_1, t_2) \equiv C(\mathbf{r}, t_1, t_2)/A(t_1, t_2)$ is a function of a *single* scaling variable τ (here the term ‘‘temporally normalized’’ reflects the property $G(\mathbf{0}, t_1, t_2) \equiv 1$). This single-parameter scaling is a peculiarity of the toy model rather than a universal rule; generally, rotational symmetry and dynamical scaling would imply that $G(\mathbf{r}, t_1, t_2)$ is a function of two variables. Finally at equal times $t_1 = t_2 = t$, both correlation functions $C(\mathbf{r}, t, t)$ and $G(\mathbf{r}, t, t)$ reduce to the equal-time correlation function $G(\tau)$ which is the function of the single scaling variable $\tau = 2t/r^4$. For the potential-free CH equation, the precise form of the equal-time correlation function $G(\tau)$ is

$$G(\tau) = \begin{cases} \frac{2\tau^{1/4}}{\Gamma(1/4)} \int_{-\infty}^\infty \cos q e^{-q^4 \tau} dq & d = 1; \\ \frac{4\tau^{1/2}}{\sqrt{\pi}} \int_0^\infty q I_0(q) e^{-q^4 \tau} dq & d = 2; \\ \frac{2\tau^{3/4}}{\Gamma(3/4)} \int_0^\infty q \sin q e^{-q^4 \tau} dq & d = 3. \end{cases}$$

8.3 Case Studies in Non-Conservative Dynamics

We now turn to explicit solutions of the basic equations of motion. Because domain interfaces in coarsening are geometrically complex, we first study the simplest settings that admit an exact analysis yet still allow for non-trivial dynamics. There are several classical such examples, such as a single domain wall and a single spherical droplet. We also discuss additional examples that are not so widely appreciated yet are rich laboratories to develop understanding. These include a single finger, a single wedge, and an isolated shrinking grain.

Straight domain wall

The simplest example of an interface is a straight domain wall. For the discrete Ising-Glauber model, this flat interface is trivial because it is merely a step function. For the continuum TDGL equation, a flat interface is a bit more interesting because the coarse-grained magnetization has a non-trivial spatial variation across the interface. Since a flat interface is stationary, the TDGL equation reduces to the ordinary differential equation for the order parameter

$$\frac{d^2 m}{dx^2} = V'(m), \quad (8.21)$$

subject to the boundary conditions $m(\pm\infty) = \pm 1$ that lead to the domain wall being stationary.

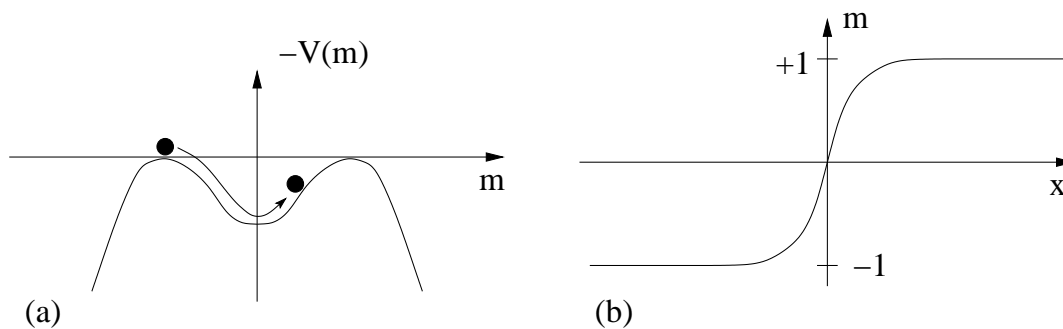


Figure 8.1: (a) The effective potential $-V(x) = -\frac{1}{2}(1 - m^2)^2$ and the motion of the analogue particle that corresponds to a single kink. The particle starts at the top of the left maximum at $m = -1$ and moves without dissipation until it eventually stops at the maximum at $m = +1$. (b) The corresponding dependence of m on x .

Before solving (8.21), we emphasize a neat interpretation of the domain wall in terms of classical mechanics: Treating x as the time variable and m as the coordinate, we see that the problem is equivalent to the motion of a fictitious, analogue unit-mass particle in the potential $-V$. The energy of this analogue particle

$$E = \frac{1}{2} \left(\frac{dm}{dx} \right)^2 - V(m) \quad (8.22)$$

does not change with “time” x . The boundary conditions imply that the total energy equals zero. Thus $\frac{dm}{dx} = \sqrt{2V(m)}$, or

$$x = \int_{m(0)}^{m(x)} \frac{d\mu}{\sqrt{2V(\mu)}}, \quad (8.23)$$

where it is customary to set the “initial condition” to be $m(x = 0) = 0$; this then corresponds to the “energy” $E = 0$. For the classic potential $V(m) = \frac{1}{2}(1 - m^2)^2$, the domain wall profile from solving (8.23) is then

$$m(x) = \tanh x. \quad (8.24)$$

This solution is known as a “kink” in a ϕ^4 theory. The width of this kink is of the order of 1, while its free energy density is

$$\frac{1}{2} \left(\frac{dm}{dx} \right)^2 + V(m) = 2V(m(x)) = \frac{1}{\cosh^4 x}, \quad (8.25)$$

and the total free energy per unit area, that is, the surface tension, is

$$\sigma = \int_{-\infty}^{\infty} 2V(m) dx = \int_{-\infty}^{\infty} 2V(m) \left(\frac{dm}{dx} \right)^{-1} dm = \int_{-1}^1 \sqrt{2V(m)} dm = \frac{4}{3}. \quad (8.26)$$

Within the classical mechanical analogy, the governing equation (8.21) can be derived by minimizing the “action”

$$\int_{-\infty}^{\infty} \left[\frac{1}{2} \left(\frac{dm}{dx} \right)^2 + V(m) \right] dx,$$

and because the kinetic and potential energies are equal, the action associated with the analogue particle coincides with the surface tension.

The mechanical analogy provides many useful insights about the phase behavior of a system in situations where an analytical description of domain walls is not feasible. For example, suppose that the initial condition is a combination of two static solutions, such as a kink-antikink configuration. That is, the order parameter starts at $m \approx -1$ for $x \rightarrow -\infty$ and increases to $m \approx +1$ over some intermediate range of x , and then returns to the value $m \approx -1$ for $x \rightarrow +\infty$. Can such a configuration be stable? Within the mechanical analogy, we are asking if it is possible for the analogue particle to start at the maximum at $m = -1$, move to the maximum at $m = +1$, and then return to the maximum at $m = -1$ (see Fig. 8.1). Clearly this motion is impossible, so we conclude without calculation that a kink-antikink pair cannot be stable. Numerical simulations show that the kink and antikink slowly move toward each other and eventually annihilate. We shall analyze this motion later in this chapter.

Another useful aspect of the mechanical analogy is that it can characterize *all* possible one-dimensional stationary solutions that correspond to a finite free energy per unit area. For any potential function, the analogue particle (i) must start at one maximum of the potential $[-V]$ at “time” $x = -\infty$ and reach another maximum of the potential $[-V]$ at $x = \infty$, and (ii) if the maxima are different, they must be adjacent. Thus for potentials with two degenerate minima (at $m = \pm 1$) there are two types of static solutions — a kink and an antikink — that we symbolically denote as $[-1, 1]$ and $[1, -1]$, respectively. Similarly for potentials with three degenerate minima (for example, a 3-state spin system with minima at $m = \pm 1$ and $m = 0$) there are four types of static solutions: $[-1, 0]$, $[0, -1]$, $[1, 0]$, $[0, 1]$. A domain wall of the form $[-1, 1]$ cannot occur. To be concrete, for the potential $V(m) = \frac{1}{2} m^2 (1 - m^2)^2$, the exact static solutions of Eq. (8.23) that separate the phases with $m = 0$ and $m = \pm 1$ are

$$m(x) = \pm (1 + e^{\pm x})^{-1/2}. \quad (8.27)$$

Higher dimensions

Perhaps the simplest interface dynamics example in higher dimension is the evolution of a small droplet of one phase with $m = -1$ in a sea of the opposite phase with $m = +1$. From the perspective of individual spins, we expect that a small cluster of minority spins will be overwhelmed by the large majority of oppositely-oriented spins. This is precisely what happens in the continuum picture. Moreover, the consideration of a small droplet avoids all the complexities associated with the tortuous interface between two competing phases, as the droplet becomes spherical as it shrinks to zero at long times.

Since the droplet shrinks, we must use the full time-dependent TDGL equation to describe its evolution. Due to spherical symmetry, the TDGL equation (8.2) simplifies to:

$$\frac{\partial m}{\partial t} = \frac{\partial^2 m}{\partial r^2} + \frac{d-1}{r} \frac{\partial m}{\partial r} - V'(m). \quad (8.28)$$

Provided that the droplet radius R greatly exceeds the interface width, we anticipate that the magnetization has the form $m(r, t) = f(r - R(t))$. Substituting this ansatz into (8.28) and defining $x = r - R(t)$ gives

$$f'' + \left(\frac{d-1}{r} + \frac{dR}{dt} \right) f' - V'(f) = 0. \quad (8.29)$$

Let's now multiply this equation by f' and integrate with respect to x through the interface. For a large droplet, the interface is relatively sharp and localized to a narrow region around a value $R(t)$. Consequently, we can set the lower limit of the integral, $-R$, to $-\infty$. This gives

$$(f')^2 \Big|_{-\infty}^{\infty} + \int_{-\infty}^{\infty} \left(\frac{d-1}{r} + \frac{dR}{dt} \right) (f')^2 dx - V(x) \Big|_{-\infty}^{\infty} = 0. \quad (8.30)$$

We now use the fact that $f(x)$ changes suddenly from -1 to 1 near $x = 0$ (corresponding to $r = R(t)$), so that f' is sharply peaked near the origin. Thus the first term vanishes. Similarly, the last term is zero, since the potential has the same value at $x = \pm\infty$. Finally, the integral is non-zero only very close to $x = 0$ and we may replace the integrand by its value at $r = R$ to give

$$\frac{d-1}{R} + \frac{dR}{dt} = 0. \quad (8.31)$$

Solving this equation gives the fundamental result that a small droplet shrinks as $R^2 = R_0^2 - 2(d-1)t$, so that the time τ for a droplet to disappear is $\tau \propto R_0^2$.

The virtue of this focus on the interfacial region is that, instead of the unsolvable TDGL equation (8.28), we obtain a more tractable equation for the interface dynamics. This simplified description of interface dynamics applies for an arbitrarily complex domain geometry, provided that the characteristic length scale associated with the interface morphology greatly exceeds the interface width. This construction is particularly simple in two dimensions. Locally an interface has a curvature $1/R$ and therefore the interface can be approximated by a circle of radius R . As a result, the velocity normal to the interface is $v \approx -1/R$. Generally in d dimensions, the interface is a $(d-1)$ -dimensional manifold and we denote by R_1, \dots, R_{d-1} its principal radii of curvature (which depend on the local position on the interface). Then the normal interface velocity is the sum of the principal curvatures $1/R_j$; this leads to the *Allen-Cahn* (AC) equation for this velocity:

$$v = -(d-1)K, \quad (8.32)$$

where K is the *mean curvature*, $K = (d-1)^{-1} \sum 1/R_j$.

There are two noteworthy points about the AC equation. First, the AC equation does not apply in one dimension, where the interface between two domains is a point. Here the interface velocity is an exponentially small function of the domain lengths on either side of the interface. This feature leads to domains that grow logarithmically in time and to extremal dynamics in which only the smallest domain merges with its neighbors in an update event. A second, more important, point is that the interface dynamics derived from the TDGL equation is an example of *curvature-driven flow*, in which general shapes evolve in arbitrary dimension due to a local velocity that is proportional to the local curvature. Curvature-driven flows have been thoroughly investigated and much is known about evolution of a single closed interface. In two dimensions, every such interface asymptotically approaches a (shrinking) circular shape. The same happens in three dimensions if the initial interface is everywhere *convex*. However, an interface that contains both convex and concave portions can fission if the concave portion of the manifold is sufficiently thin, such as an elongated liquid drop with an extremely thin neck of fluid in the middle. The classification of all possible topology changes in higher dimensions due to curvature-driven flow is still incomplete.

Two-dimensional unbounded domains

A beautiful set of domain evolution problems is inspired by returning to a discrete Ising spin system on the square lattice and asking: what are the simplest initial states for which evolution under zero-temperature Glauber dynamics can be studied analytically? A example that is too simple because it is static is a single straight domain wall that cuts a finite system in two. To have a system that actually evolves, the initial interface must contain at least one corner and we now study two such examples (Fig. 8.2): (a) the semi-infinite finger (2 initial corners), and (b) the 90° infinite wedge (1 initial corner). Curiously, although the finger appears to be more complex than the wedge because there are two initial corners, its dynamics is simpler than that of the wedge. The wedge is, in fact, extremely rich, with nice connections between the shape of the wedge and the famous number theoretic-problem of partitioning of the integers.

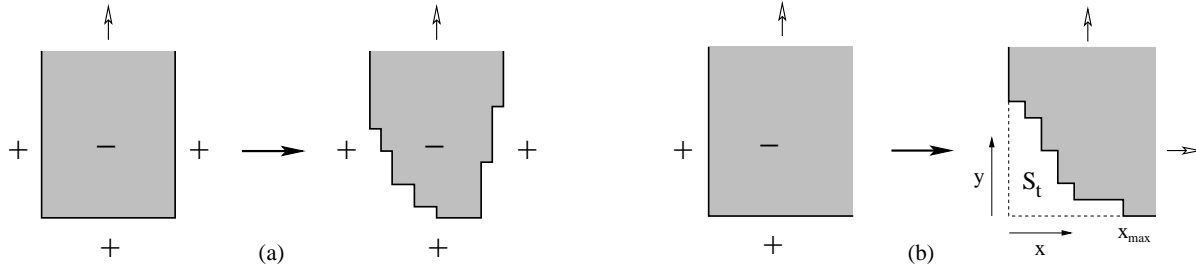


Figure 8.2: (a) A semi-infinite finger and (b) a 90° infinite wedge, showing both the initial state (left of each figure) and the system at a later time (right side). For the wedge, the evolving interface encloses an area S_t at time t .

Let's begin with the semi-infinite finger. At the individual spin level, the interface develops a series of terraces that culminate at the tip. At the tip isolated islands can even pinch off. A detailed understanding of these microscopic details has yet to be achieved. However, within the continuum description the asymptotic behavior is quite simple. Let the minority phase initially occupy the semi-infinite region $y > 0$ and $|x| < L$. The interesting limit is $t \gg L^2$ where sufficient time has elapsed so that the two corners of the initial finger interact. In this long-time regime, the finger relaxes to a limiting shape that recedes at a constant velocity. In a reference frame that moves with the finger, the interface $y(x)$ is then stationary.

For this geometry, the AC equation is

$$v_n = \frac{y''}{[1 + (y')^2]^{3/2}}. \quad (8.33)$$

Here v_n is the velocity normal to the interface. The right-hand side is just the curvature of the locus $y(x)$ that defines the finger boundary and the prime denotes differentiation with respect to x . In the steady state, only the vertical component of the velocity, given by $v_y = v_n / \cos \theta = v_n \sqrt{1 + (y')^2}$, is relevant (see Fig. 8.3). Thus the vertical velocity satisfies the equation

$$v_y = \frac{y''}{1 + (y')^2}, \quad (8.34)$$

subject to the boundary condition $y \rightarrow \infty$ when $|x| \rightarrow L$. The solution to this equation is

$$y = -\frac{2L}{\pi} \ln \left[\cos \left(\frac{\pi x}{2L} \right) \right]. \quad (8.35)$$

Substituting this profile into Eq. (8.34), we find that the finger recedes at a constant velocity $v = \pi/2L$.

Next we study the infinite wedge (Fig. 8.2). For concreteness, let the corner be at the origin so that the wedge initially occupies the region $x, y \geq 0$. The corner of the wedge recedes diffusively, $x, y \propto \sqrt{t}$, both in Ising-Glauber dynamics and in the continuum description. Because of the absence of any constant with dimension of length in Eq. (8.34), the corresponding solution admits the self-similar form

$$X = x(t)/\sqrt{t}, \quad Y(X) = y(x, t)/\sqrt{t}, \quad (8.36)$$

Notice that the increase of the magnetization is equal to twice the area under the curve $y(x, t)$. From (8.36), the area is proportional to t , so that the magnetization also grows linearly with time. To determine the evolution of the wedge, we substitute the ansatz Eq. (8.36) into the equation of motion (8.34) and find that the scaling function $Y(X)$ obeys

$$\frac{Y - XY'}{2} = \frac{Y''}{1 + (Y')^2}, \quad (8.37)$$

where prime indicates differentiation with respect to X . Equation (8.37) should be solved subject to the constraints $\lim_{X \rightarrow \infty} Y(X) = 0$ and $\lim_{X \rightarrow +0} Y(X) = \infty$ that correspond to the wedge geometry. A wedge that initially occupies the region $y > |x| \tan \theta$ could also be studied if we impose the constraints $Y \rightarrow \pm X \tan \theta$ as $X \rightarrow \pm \infty$.

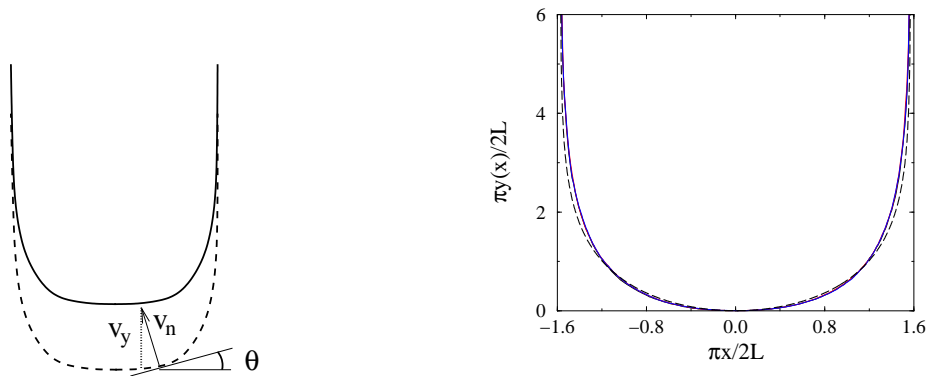


Figure 8.3: (Left) Schematic illustration of the receding finger, showing the normal velocity v_n and the vertical velocity v_y . (Right) Comparison of the finger shape predicted by the TDGL approach given in Eq. 8.35 (dashed) with simulation results for a system of width $2L = 400$ at long times (solid).

We introduce the polar coordinates $(X, Y) = (r \cos \theta, r \sin \theta)$ to recast Eq. (8.37) into the following equation for $r = r(\theta)$:

$$2r \frac{d^2 r}{d\theta^2} - (4 + r^2) \left(\frac{dr}{d\theta} \right)^2 = r^2 (2 + r^2). \quad (8.38)$$

Writing $\frac{dr}{d\theta} = R(r)$, reduces Eq. (8.38) to a first-order equation whose solution is $R^2 = r^4 e^{r^2/2} F(r, r_0)$, with

$$F(r, r_0) = \int_{r_0}^r \left(\frac{2}{\rho^3} + \frac{1}{\rho} \right) e^{-\rho^2/2} d\rho, \quad (8.39)$$

and r_0 is the scaled distance from the origin to the closest point on the interface. The interface is now determined from

$$\frac{dr}{d\theta} = \pm r^2 e^{r^2/4} \sqrt{F(r, r_0)}, \quad (8.40)$$

with the plus sign for $\theta \geq \pi/4$ and the minus sign for $\theta \leq \pi/4$ to give a symmetric solution about the diagonal $\theta < \pi/4$. Integrating Eq. (8.40) gives the explicit equation for $\theta = \theta(r)$

$$\theta = \int_r^\infty \rho^{-2} e^{-\rho^2/4} [F(\rho, r_0)]^{-1/2} d\rho \quad (8.41)$$

for $\theta \leq \pi/4$. For $\pi/4 < \theta < \pi/2$, we simply use $r(\theta) = r(\frac{\pi}{2} - \theta)$ to ensure symmetry of the interface about the diagonal. The value of the unknown r_0 may now be obtained by ensuring that $\theta = \pi/4$ when $r = r_0$. This gives the criterion

$$\int_{r_0}^\infty r^{-2} e^{-r^2/4} [F(r, r_0)]^{-1/2} = \frac{\pi}{4} dr, \quad (8.42)$$

whose numerical solution is $r_0 \approx 1.0445$. Equation (8.41), with F given by (8.39), provides an explicit representation of $\theta(r)$ on the interface in terms of the (scaled) distance $r \in [r_0, \infty)$ from the origin. For $r \rightarrow \infty$, the interface becomes much simpler. From Eqs. (8.39) and (8.41) we obtain $\theta \rightarrow A r^{-3} e^{-r^2/4}$ with $A = 2 [F(\infty, r_0)]^{-1/2}$ which, in Cartesian coordinates, is

$$Y \rightarrow A X^{-2} e^{-X^2/4}. \quad (8.43)$$

Apart from the numerical factor A , the asymptotic behavior follows directly from Eq. (8.37) after dropping the subdominant terms.

The staircase profile of the interface in Fig. 8.2(b) has a simple relation to the famous number-theoretic problem of the partitions of the integers. Given an arbitrary integer N , how many different ways can we break up this number into k integer pieces n_1, n_2, \dots, n_k with $\sum_k n_k = N$? Geometrically, this question is

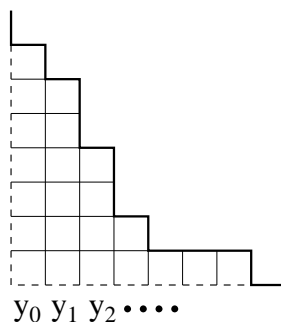


Figure 8.4: The Young diagram that is based on the interface profile of Fig. 8.2. This diagram corresponds to a partition of the integer 22 into the set $\{7, 6, 4, 2, 1, 1, 1\}$.

the same as enumerating all possible interfaces with a given number of flipped spins in the wedge geometry! The interface height y_k and the k^{th} column is same as n_k in the partitioning problem. For $N \rightarrow \infty$, the staircase generated by its partition approaches a limiting shape. The equation for this shape is remarkably simple:

$$e^{-\lambda x} + e^{-\lambda y} = 1, \quad \text{with } \lambda = \frac{\pi}{6\sqrt{N}}. \quad (8.44)$$

In scaled units, the asymptotic shape of the integer partition limiting staircase is $Y \sim \frac{\sqrt{6}}{\pi} e^{-\pi X/\sqrt{6}}$, whereas the asymptotic Ising staircase is given by $Y \sim \frac{1.0445\dots}{X^2} e^{-X^2/4}$. The existence of two distinct shapes arises from the different construction rules of the Ising interface and the interface generated by the integer partitions. In the partitioning of the integers, each staircase corresponding to fixed N is generated with the same weight. On the other hand, the Ising interface is generated dynamically and when its area reaches N , the interface contains an imprint of its entire history.

8.4 Conservative Dynamics

The influence of a conservation law severely limits the way in which an interface between two domains can move. While an interface should move to reduce its local curvature and consequently the energy, such an evolution has to be accompanied by a global rearrangement of interfaces to ensure that the order parameter is conserved. While the full problem remains quite open, much progress has again been made in studying the simplest geometries, such as a single droplet or a dilute population of droplets immersed in a majority phase. Here, each droplet remains spherical throughout the evolution, so that one avoids the geometrical complexity associated with random interfaces. Nevertheless, the kinetics of this dilute limit is still quite subtle and rich.

Evolution of a single droplet

As an essential preliminary, consider the evolution of a single droplet of one phase that is immersed in a background of the opposite phase. This statement, however, has a basic inconsistency that requires clarification. If the two phases were perfectly separated, then the droplet could not evolve because any change in the droplet size would violate the conservation of the order parameter. Instead, we should think of a single drop of liquid that is floating in a closed container of gas that is saturated with the liquid in the vapor phase. At the surface of the droplet there is both evaporation as well as condensation of vapor molecules back into the droplet. It is through the combination of these two processes that the droplet can evolve while still conserving the order parameters.

The condensation rate is given by the flux of vapor molecules to the droplet which, in turn, is determined by vapor concentration in the gas. In principle, the vapor concentration exterior to the droplet obeys the diffusion equation. However, because the droplet radius changes slowly with time, we apply the quasi-static approximation (see Sec. 2.5) in which we ignore the time dependence and deal with the much simpler

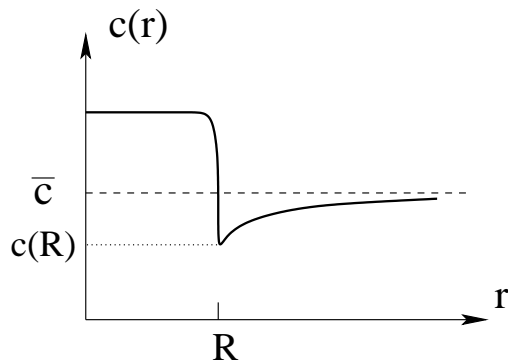


Figure 8.5: Dependence of the concentration of the minority phase as a function of radius.

Laplace equation to determine the external vapor concentration. Schematically, the concentration of the minority phase as a function of distance from the center of a droplet of radius R should then have the dependence sketched in Fig. 8.5. The average concentration of the minority phase in the entire system \bar{c} must be larger than the supersaturation value c_∞ , *i.e.*, there must be supersaturation, so that a droplet can form in the first place. (Conversely, for $\bar{c} < c_\infty$, the minority phase remains as a homogeneous vapor in the gas.) Inside the droplet, the concentration is much higher than \bar{c} by the very definition of a droplet. Outside the droplet, the vapor concentration obeys Laplace's equation with the boundary conditions $c(r \rightarrow \infty) \rightarrow \bar{c}$ and $c(R)$ determined by the Gibbs-Thompson relation (see below). In three dimensions, $c(r)$ therefore has the dependence

$$c(r) = \bar{c} - [\bar{c} - c(R)] \frac{R}{r}. \quad (8.45)$$

The Gibbs-Thompson relation relates $c(R)$ to c_∞ by the following physical picture: for a bulk liquid in equilibrium with a saturated vapor, the vapor concentration at the interface must be c_∞ by definition. For a small droplet, the vapor concentration is larger than that of a bulk liquid because a larger fraction of molecules are at the interface. Thus $c(R)$ should exceed c_∞ by an amount that vanishes as the droplet radius goes to infinity. This relationship is encapsulated by the Gibbs-Thompson relation $c(R) = c_\infty \left(1 + \frac{\nu}{R}\right)$, where ν is known as the capillary length and is simply related to the surface tension and the temperature.

Assembling these elements, the volume V of an isolated droplet changes with rate

$$\frac{dV}{dt} = 4\pi R^2 \frac{dR}{dt} = 4\pi R^2 D \left. \frac{\partial c}{\partial r} \right|_{r=R}, \quad (8.46)$$

from which $\dot{R} = D[\bar{c} - c(R)]/R$. We now define $\Delta = \bar{c} - c_\infty$ as the degree of supersaturation, and use the Gibbs-Thompson relation to eliminate $c(R)$ in (8.46) to give

$$\frac{dR}{dt} = \frac{D}{R} \left(\Delta - c_\infty \frac{\nu}{R} \right) \equiv \frac{\alpha}{R^2} \left(\frac{R}{R_c} - 1 \right). \quad (8.47)$$

From the latter form, it is clear that for $R > R_c = c_\infty \nu / \Delta$ the droplet grows, while for $R < R_c$ the droplet shrinks. More importantly, we see by power counting that this equation contains the seeds of $t^{1/3}$ coarsening. An isolated supercritical droplet asymptotically grows as $t^{1/3}$, while a subcritical droplet shrinks to zero size in a time that scales as the cube root of its initial radius.

Lifshitz-Slyazov-Wagner coarsening

The foregoing discussion provides the basis for understanding the coarsening of a dilute heterogeneous population of droplets in a supersaturated background. This problem was independently analyzed by Lifshitz and Slyozov, and by Wagner, and we refer to the problem as LSW coarsening. The dilute limit allows us to make the approximation that droplets are non-interacting so that the concentration field around each droplet is the same as that of an isolated droplet. The basic feature of this coarsening is already contained in Eq. (8.47): droplets whose radii is larger than R_c grow and those with smaller radii shrink. In a population

of heterogeneous droplets, the value of R_c has to be determined self consistently, and we show that this calculation gives $R_c \propto t^{1/3}$.

Let $f(R, t)$, be the concentration of droplets of radius R at time t . This concentration evolves by the continuity equation

$$\frac{\partial f}{\partial t} + \frac{\partial j}{\partial R} = 0, \quad (8.48)$$

where the flux $j = \dot{R}f(R, t)$ is just the difference between the increase and decrease of droplets of radius R due to their evolution. We wish to solve this equation of motion with \dot{R} given by Eq. (8.47) and subject to the constraint that the total mass of the minority phase is conserved. This constraint may be written as

$$\bar{c} - c_\infty + \frac{4\pi}{3} \int_0^\infty R^3 f(R, t) dR = \text{const.} \quad (8.49)$$

In the minority limit, the volume fraction of the minority phase that exists as freely diffusing monomers is vanishingly small. Thus the conservation law reduces to the condition that the total volume of the droplets is fixed. With this proviso, Eqs. (8.47)–(8.49) constitute the governing equations of coarsening in the minority limit with a conserved order parameter.

To solve these equations of coarsening, it is again very useful to apply scaling. The natural scaling ansatz for this system, under the assumption that the mass of all droplets is conserved, is

$$f(R, t) = \frac{1}{R_c^4} \phi\left(\frac{R}{R_c}\right).$$

Here the prefactor is determined by the conservation of the total mass of the minority phase, namely, $\int R^3 f(R, t) dR = \text{const.}$ Substituting this scaling ansatz into (8.48), the first term in this equation becomes

$$\frac{\partial f}{\partial t} = -\frac{4\dot{R}_c}{R_c^5} \phi - \frac{1}{R_c^4} \phi' \frac{R\dot{R}_c}{R_c^2} = -\frac{\dot{R}_c}{R_c^5} (4\phi + z\phi'),$$

where the prime denotes differentiation with respect to the scaled variable $z \equiv R/R_c$. Similarly, the second term in (8.48) becomes

$$\frac{\partial}{\partial R} \left[\frac{\alpha}{R^2} \left(\frac{R}{R_c} - 1 \right) \frac{1}{R_c^4} \phi \right] = \frac{\alpha}{R_c^7} \left[\left(\frac{1}{z} - \frac{1}{z^2} \right) \phi' + \left(\frac{2}{z^3} - \frac{1}{z^2} \right) \phi \right].$$

With these preliminaries the partial differential equation of (8.48) is converted into the ordinary differential equation

$$R_c^2 \dot{R}_c = \alpha \frac{\left[\left(\frac{1}{z} - \frac{1}{z^2} \right) \phi' + \left(\frac{2}{z^3} - \frac{1}{z^2} \right) \phi \right]}{4\phi + z\phi'} \equiv \alpha\gamma, \quad (8.50)$$

where we rearranged the terms to put all the time dependence of the left and all the z dependence on the right. Since both sides are functions of different variables they each must be constant. In the simplest applications of scaling, such as the scaling solution to the diffusion equation in Sec. 1.1, the value of the separation constant plays little role in the scaling solution. In contrast, for coarsening, the separation constant γ is essential. Depending on the value of γ , there are three different regimes of behavior, only one of which is physically meaningful.

Let us now examine the separated equations and thus determine the condition that gives the physical value of γ . For the time dependence we have

$$R_c^2 \dot{R}_c = \alpha\gamma, \quad (8.51)$$

with solution

$$R_c(t) = (3\alpha\gamma t)^{1/3}. \quad (8.52)$$

Thus coarsening under the constraint of a conserved order parameter leads to a $t^{1/3}$ growth of the typical droplet radius. This slower-than-diffusive growth of the typical droplet also justifies for the quasi-static

approximation that was used to determine the concentration outside a droplet. For the z dependence of the scaling function, the governing equation (8.50) becomes, after some simple rearrangement:

$$a\phi' + b\phi = 0, \quad \text{with} \quad a = -\frac{1}{z^2} + \frac{1}{z} - z\gamma, \quad b = \frac{2}{z^3} - \frac{1}{z^2} - 4\gamma. \quad (8.53)$$

Thus the scaling function is formally given by

$$\ln \phi = \int^z -\frac{b(y)}{a(y)} dy = \int^z \frac{2-y-4\gamma y^3}{1-y+\gamma y^3} \frac{dy}{y}. \quad (8.54)$$

Thus far, the reasoning is standard: we've used scaling to separate the partial differential equation (8.48) into two ordinary differential equations. As is generally the case, the time dependence then follows easily. For LSW coarsening, the analysis of the z dependence is subtle because of the essential role of the separation constant γ . The first basic and somewhat surprising consequence of Eq. (8.54) is that $\phi(z)$ must have a sharp cutoff at a value z_{\max} , beyond which $\phi(z) = 0$. To demonstrate this fact, suppose the opposite is true. Then as $z \rightarrow \infty$, Eq. (8.54) would tell us that $\phi(z)$ should asymptotically vary as

$$\ln \phi \sim \int^z -4 \frac{dy}{y} \sim -4 \ln z \longrightarrow \phi \sim z^{-4}.$$

A power law tail for ϕ is impossible, however, as this asymptotic decay would lead to a divergence of the total mass of the minority phase:

$$\int R^3 \phi(R, t) dR \sim \int z^3 z^{-4} dz \rightarrow \infty.$$

Thus we conclude that $\phi(z)$ has a sharp cutoff beyond some value z_{\max} .

A second and more profound fact is that only one value of the separation constant γ is physically allowed. To see why this is the case, let's re-examine the behavior of \dot{R} in scaled units. Using Eqs. (8.47) and (8.51), we find, after some simple algebra:

$$\dot{z} = \frac{1}{3\gamma t} \left(\frac{1}{z} - \frac{1}{z^2} - \gamma z \right) \equiv \frac{1}{3\gamma t} g(z). \quad (8.55)$$

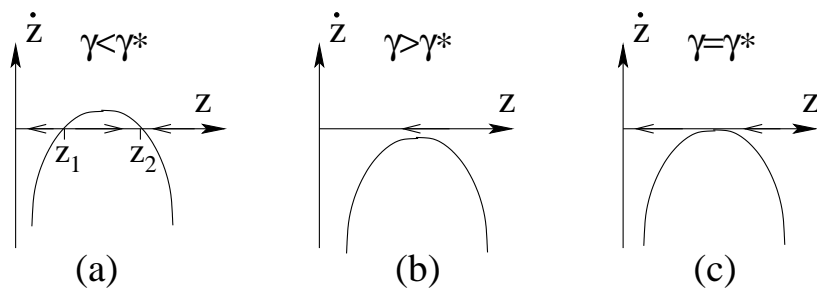


Figure 8.6: Sketch of $\dot{z} = g(z)/(3\gamma t)$ versus z for the 3 cases: (a) $\gamma < \gamma^*$, (b) $\gamma > \gamma^*$, and (c) $\gamma = \gamma^*$. The arrows on the z -axis shows the flow of z in Eq. (8.55).

Let's now examine the behavior of $g(z)$ for different values of γ . There are 3 cases:

- (a) $\gamma < \gamma^* = 4/27$. Here $z(t)$ flows exponentially quickly to the stable fixed point at z_2 for $z(0) > z_1$ (Fig. 8.6). That is, the radii of all droplets approach the common value $R_c z_2$, which diverges as $t \rightarrow \infty$. Such a distribution cannot satisfy mass conservation.
- (b) $\gamma > \gamma^*$. Here $z(t) \rightarrow 0$ exponentially quickly in time for any initial value of z . Thus all droplets shrink to zero and mass conservation is again violated.

- (c) $\gamma = \gamma^*$. In this case $z = 3/2$ is a fixed point, but one that is approached as a power law in time. This subtle behavior is the mechanism that allows mass conservation to be satisfied. If the fixed point at $z = 3/2$ was reached exponentially quickly, then again all droplet radii would approach the common value of $3R_c/2$ and mass conservation would be violated. The slow decrease in z ensures the delicate balance between growth and shrinking of clusters in a mass-conserving way.

For the physical case of $\gamma = \gamma^*$, Eq. (8.54) for the scaling function can be factorized as

$$\ln \phi = \int^z \frac{2 - y - \frac{16}{27}y^3}{(y - \frac{3}{3})^2(y + 3)} \frac{dy}{y}.$$

Evaluating the latter integral by a partial fraction expansion now gives the quite complex form of the scaling function (in three dimensions):

$$\begin{aligned} \phi(z) &\propto z^2 (z + 3)^{-7/3} (3 - 2z)^{-11/3} e^{-3/(3-2z)} & z < 3/2; \\ &= 0 & z > 3/2, \end{aligned} \tag{8.56}$$

and a plot of this scaled droplet radius distribution is shown in Fig. 8.7.

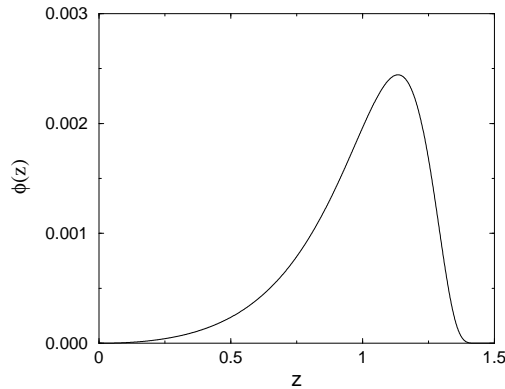


Figure 8.7: The scaling function $\phi(z)$ for LSW coarsening given by Eq. (8.56).

8.5 Extremal Dynamics

Shrinking of a single domain

While power-law domain growth is a generic feature of zero-temperature coarsening, there is one important case where much slower logarithmic growth occurs — the TDGL equation in one dimension. The case of one dimension is special because there is no local curvature to drive an interface; rather the interface moves by a net flux of order parameter across neighboring domains that is determined, in turn, by their lengths. In the long-time limit, this flux vanishes as e^{-L} , where L is the length of a typical domain; the smallness of this flux is responsible for logarithmic coarsening. As a consequence of this slow growth, the asymptotic dynamics of the one-dimensional TDGL equation has an extremal character in which only the smallest domain in the system merges with its two nearest neighbors in a single update state. This extremal picture then provides a natural way to determine the domain dynamics.

To understand the origin of the slow domain growth, consider a single large domain of length $L = x_2 - x_1$ of magnetization is close to $+1$ that is immersed in a sea with the magnetization close to -1 (Fig. 8.8). The two interfaces of this bubble consist of a kink at $x = x_1(t)$ and an antikink at $x = x_2(t) = x_1 + L$. If L is much larger than the width of each interface, which is a good approximation at long times, the kink and

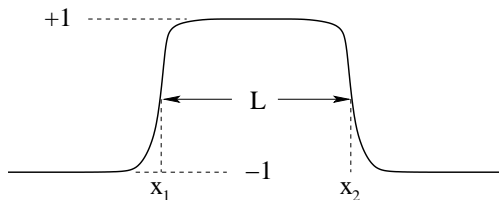


Figure 8.8: A single domain with magnetization close to +1 in a background where the magnetization is close to -1.

antikink are nearly independent. Under this assumption, the spatial dependence of the order parameter is, using Eq. (8.24),

$$m(x, t) \approx \tanh(x - x_1(t)) - \tanh(x - x_2(t)) - 1. \quad (8.57)$$

Let's now estimate how the interfaces move for this kink/antikink pair. Substituting the profile (8.57) into the TDGL equation (8.2) and keeping only the lowest-order terms, we find that asymptotically

$$\dot{x}_1 = -\dot{x}_2 \approx e^{-2(x_2 - x_1)}. \quad (8.58)$$

Consequently the domain length $L = x_2 - x_1$ shrinks according to $\dot{L} \approx -2e^{-2L}$ which gives $L(t) = \frac{1}{2} \ln [e^{2L(0)} - 4t]$, while the time for the domain to disappear is $\tau = \frac{1}{4}e^{2L(0)}$.

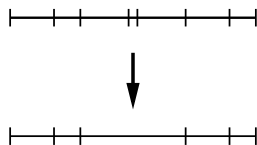


Figure 8.9: Extremal dynamics. The shortest domain merges with its two neighbors, while all other domains remain static.

This exponential length dependence of the shrinking time has profound consequences for the evolution of a heterogeneous domain array in one dimension. In the long-time limit, the shrinking time of the smallest domain is orders of magnitude shorter than that of the next smallest domain. As a result, the order in which domains merge with their neighbors becomes deterministic. This length ordering leads to the following simple extremal dynamics for TDGL domain evolution: (i) pick the smallest domain and merge it with its two nearest neighbors while keeping all other domains fixed; (ii) repeat *ad infinitum* (Fig. 8.9).

The domain length distribution

We now study how the domain length distribution evolves by this extremal dynamics. For simplicity, we assume that the total initial magnetization vanishes, so that the average length of domains of positive and negative magnetization are equal. The ensuing extremal dynamics coarsening resembles the Swendsen-Wang and Wolff cluster dynamics that were discussed in Sec. 7.5. However, in extremal dynamics, the natural time-like variable is the length ℓ of the shortest domain. Our goal is to determine $c(x, \ell)$, the density of domains of length x when the shortest domain has length ℓ . We choose the initial domain lengths from a continuous distribution so that each domain has a distinct length. The total density of domains is $\rho = \int_{\ell}^{\infty} c(x, \ell) dx$ and by definition $\int_{\ell}^{\infty} x c(x, \ell) dx = 1$.

Let's first show how the shortest domain plays the role of a time-like variable. When the shortest domain has length ℓ , suppose that a certain number of mergings occur so that all domains with lengths in the range $(\ell, \ell + \Delta\ell)$ merge with their neighbors so that the length of the shortest domain increases from ℓ to $\ell + \Delta\ell$. The density of the domains in this length range is $c(\ell, \ell)\Delta\ell$. Since there is a net loss of two domains in each merger, $\rho(\ell + \Delta\ell) = \rho(\ell) - 2c(\ell, \ell)\Delta\ell$. Thus the domain density obeys

$$\frac{d\rho}{d\ell} = -2c(\ell), \quad (8.59)$$

and in this rate equation the minimal length ℓ plays the role of a time.

The master equation for the domain length distribution may now be written in terms of this time-like variable. When the length of the shortest domain increases from ℓ to $\ell + \Delta\ell$, the length distribution $c(x, \ell)$ changes as follows:

$$c(x, \ell + \Delta\ell) - c(x, \ell) = \left[-2 \frac{c(x, \ell)}{\rho} + \Theta(x - 3\ell) \int_{\ell}^{x-2\ell} \frac{c(y, \ell)}{\rho} \frac{c(x - \ell - y, \ell)}{\rho} dy \right] c(\ell, \ell) \Delta\ell. \quad (8.60)$$

The first term on the right accounts for the loss of a domain of length x due to its merging. The factor of 2 stems from the fact that a domain of length x can be either to the left or to the right of the minimal domain. The second term accounts for the gain of a domain of length x due to the merging of three domains of lengths ℓ , y , and $x - \ell - y$. The Heaviside step function $\Theta(x - 3\ell)$ enforces the condition that when the smallest domain has length ℓ , the smallest domain that can be created by merging must have length equal to at least 3ℓ . The last factor $c(\ell, \ell)\Delta\ell$ counts the number of merging events that occur as the minimal size increases from ℓ to $\ell + \Delta\ell$.

In close analogy with the discussion of cluster dynamics in Sec. 7.5, a remarkable feature of extremal evolution is that if the domains are initially uncorrelated, they remain uncorrelated at all times. Merging of domains do not affect their neighbors, nor are domains affected by their neighbors. Therefore the domain length distribution evolves according to the exact equation

$$\frac{dc(x, \ell)}{d\ell} = c(\ell, \ell) \left[-2 \frac{c(x, \ell)}{\rho} + \Theta(x - 3\ell) \int_{\ell}^{x-2\ell} \frac{c(y, \ell)}{\rho} \frac{c(x - \ell - y, \ell)}{\rho} dy \right] \quad (8.61)$$

for $x > \ell$. At this point, it is again convenient to introduce the normalized length density $P(x, \ell) = c(x, \ell)/\rho$ whose governing equation includes only the gain term:

$$\frac{dP(x, \ell)}{d\ell} = \Theta(x - 3\ell) P(\ell, \ell) \int_{\ell}^{x-2\ell} P(y, \ell) P(x - \ell - y, \ell) dy. \quad (8.62)$$

Let's now investigate the asymptotic behavior of the domain length distribution. The ever-growing minimal domain length ℓ defines a basic scale, and we postulate that ℓ is the only length scale in the long time limit. Thus we assume that $P(x, \ell)$ approaches the scaling form

$$P(x, \ell) \simeq \ell^{-1} \Phi(x\ell^{-1}) \quad (8.63)$$

as $\ell \rightarrow \infty$, where the prefactor is fixed by the normalization condition $\int_1^{\infty} P(x, \ell) dx = 1$. As a result, the scaling function must satisfy the normalization condition $\int_1^{\infty} \Phi(z) dz = 1$. Substituting the scaling ansatz for $P(x, \ell)$ into the master equation (8.62), the scaling function obeys the nonlinear integro-differential equation

$$z \frac{d\Phi(z)}{dz} + \Phi(z) + \Theta(z - 3) \Phi(1) \int_1^{z-2} \Phi(y) \Phi(z - 1 - y) dy = 0. \quad (8.64)$$

Given that the master equation involves a convolution, we again study the master equation in the Laplace domain. Here we introduce the Laplace transform $\phi(s) = \int_1^{\infty} \Phi(z) e^{-sz} dz$ with the lower limit of 1 because the convolution has this same lower limit. Multiplying (8.64) by e^{-sz} and integrating by parts, the Laplace transform then obeys the ordinary differential equation

$$s \frac{d\phi}{ds} = -\Phi(1) (1 - \phi^2) e^{-s}, \quad (8.65)$$

with the boundary condition $\phi(0) = 1$. Expanding $\phi(s) = 1 + s\phi'(0)$ on the right hand side and evaluating the equality at $s = 0$ yields the normalized density of the shortest domains $\Phi(1) = 1/2$. Consequently, the asymptotic density of the shortest domains is given by

$$P(\ell) \simeq (2\ell)^{-1}. \quad (8.66)$$

Substituting $\Phi(1) = \frac{1}{2}$ into (8.65) and solving this equation yields the Laplace transform

$$\phi(s) = \tanh [\text{Ei}(s)/2], \quad (8.67)$$

where $\text{Ei}(x)$ is the exponential integral $\text{Ei}(x) \equiv \int_x^\infty \frac{1}{u} e^{-u} du$.

The average domain length, $\langle x \rangle \simeq \langle z \rangle \ell$, follows from the small-argument behavior $\phi(s) \approx 1 - s\langle z \rangle$ and the asymptotic properties of the exponential integral¹ to give

$$\langle x \rangle \simeq 2e^\gamma \ell. \quad (8.68)$$

The ratio between the average length and minimal domain length approaches $2e^\gamma = 3.562144$. The conservation law $\rho\langle x \rangle = 1$ then gives the total domain density $\rho \simeq \frac{1}{2}e^{-2\gamma}\ell^{-1}$. Indeed, the density satisfies (8.59) $\frac{d\rho}{d\ell} = -2P(\ell)\rho \simeq \rho/\ell$.

Extremal properties of the domain distribution can be evaluated directly from the integro-differential equation (8.64). In the length range $1 < z < 3$, the integral drops out. The scaling function obeys the differential equation $z\frac{d}{dz}\Phi(z) = -\Phi(z)$ with the boundary condition $\Phi(1) = 1/2$, so

$$\Phi(z) = (2z)^{-1}, \quad 1 \leq z \leq 3. \quad (8.69)$$

Interestingly, the normalized domain density becomes time-independent, $P(x, \ell) \rightarrow (2x)^{-1}$, in the (time-dependent) range $\ell < x < 3\ell$.

add exponential tail of distribution

The scaling analysis employed effectively resets the length of shortest domain to one after each merger. The similarity solution can be viewed as a *fixed-point* of this renormalization procedure. This technique is sometime termed *real space renormalization* or *strong disorder renormalization*.

Section on persistence has been temporarily commented out.

Also the subsection on the autocorrelation function has been commented out.

8.6 Nucleation and Growth

Nucleation-and-growth processes² are useful for modeling a remarkable wealth of phenomena. In this process, size-less islands (seeds) nucleate with a spatially-homogeneous rate $\gamma(t)$. The shape of the islands is spherical and their radius is $r(s)$ where s is the island lifetime. A point in space may be covered by multiple islands (figure 8.10).

Eventually, space becomes completely filled. The volume fraction, $\rho(t)$, the fraction of space covered by islands, can be calculated exactly. Its complement, $1 - \rho(t)$, the fraction of uncovered space, is the probability that a given point in space, say the origin, remains uncovered at time t . For the origin to remain uncovered, no nucleation events may occur at a distance smaller than $r(t - \tau)$ from the origin at all times $\tau < t$; the corresponding volume is $V(t - \tau) = V_d[r(t - \tau)]^d$ with $V_d = \pi^{d/2}/\Gamma(1 + d/2)$ the volume of the d -dimensional unit hypersphere. Since the nucleation process is random, the probability that no nucleation events occur in all of these volumes is

$$1 - \rho(t) = \exp \left[- \int_0^t d\tau \gamma(\tau) V(t - \tau) \right]. \quad (8.70)$$

There are two important special cases: (i) Homogeneous nucleation where the nucleation rate is constant, $\gamma(t) = \gamma$; (ii) Instantaneous nucleation where all nucleation seeds appear at the same time, $\gamma(t) = \sigma\delta(t)$. For a constant growth velocity, $dr/dt = v$, the uncovered fractions are

$$1 - \rho(t) = \begin{cases} \exp[-\gamma U_d v^d t^{d+1}] & \text{homogeneous nucleation;} \\ \exp[-\sigma V_d (vt)^d] & \text{instantaneous nucleation.} \end{cases} \quad (8.71)$$

Here, $U_d = V_d/(d + 1)$. The argument of the exponential equals the nucleation rate times the “excluded” volume, i.e., the volume of the space-time (\mathbf{y}, τ) region where nucleation events affect the origin $(\mathbf{0}, t)$. For homogeneous nucleation, this region is a d -dimensional hyper-cone of radius $v_0 t$ and height t ; namely, a

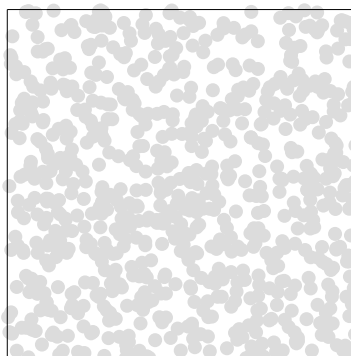


Figure 8.10: Nucleation-and-growth in two-dimensions (instantaneous nucleation).

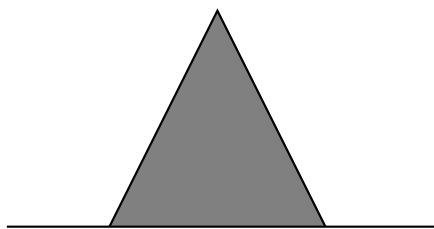


Figure 8.11: Homogeneous nucleation-and-growth in one-dimension. For a point to remain uncovered, no nucleation events may occur in a spacetime triangle.

triangle in one-dimension (Fig. 8.11), a cone in two-dimensions, etc. For instantaneous nucleation, the exclusion region is a d -dimensional sphere of radius $v_0 t$.

Multiple-point correlation functions can be calculated as well. To distinguish the covered phase from the uncovered one, we introduce the phase parameter

$$\phi(\mathbf{x}, t) = \begin{cases} 1 & \text{if uncovered} \\ 0 & \text{if covered.} \end{cases} \quad (8.72)$$

The multiple-point correlation function $G_n(\mathbf{x}_1, \dots, \mathbf{x}_n; t) = \langle \phi(\mathbf{x}_1, t) \cdots \phi(\mathbf{x}_n, t) \rangle$ equals the probability that all n points \mathbf{x}_i remain uncovered at time t . This probability is evaluated following the very same reasoning used to evaluate the uncovered fraction. One should ensure that all nucleation events that can lead to covering of any of these points do not occur. The multiple point correlation function is

$$G_n(\mathbf{x}_1, \dots, \mathbf{x}_n; t) = \exp \left\{ - \int d\mathbf{y} \int_0^t d\tau \gamma(\tau) \left[1 - \prod_{i=1}^n \Theta(|\mathbf{x}_i - \mathbf{y}| - r(t - \tau)) \right] \right\}, \quad (8.73)$$

¹For small- x , $\text{Ei}(x) \simeq -\gamma - \ln x$ with $\gamma = 0.577215$ the Euler constant.

²This process is referred to as the Kolmogorov-Avrami-Johnson-Mehl or KAJM process.

where $\Theta(x)$ is the Heaviside step function; $\Theta(x) = 1$ for $x > 0$ and $\Theta(x) = 0$ for $x < 0$. The integration is over all possible nucleation sites \mathbf{y} and nucleation times τ with the appropriate measure, the nucleation rate $\gamma(\tau)$. The integrand is zero when none of the points \mathbf{x}_i are affected by a nucleation event at (\mathbf{y}, τ) . It equals one when at least one of the points \mathbf{x}_i would become covered due to nucleation at (\mathbf{y}, τ) . We check that the one-point function $G_1(t) = G_1(\mathbf{x}, t) = 1 - \rho$ agrees with (8.70): $G_1(t) \equiv \exp[-\int_0^t d\tau \gamma(\tau) \int_{\mathbf{y} < r(t-\tau)} d\mathbf{y}]$; the spatial integral yields $V(t-\tau)$. The crucial feature that allows us to obtain the correlators is that nucleation events are uncorrelated, neither in space, nor in time.

In what follows, we consider constant growth velocities $dr/dt = v_0$. When all pairs of points are separated by distances larger than $2v_0t$, the integral (8.73) separates into n non-overlapping integrals, and the correlation function factorizes

$$G_n(\mathbf{x}_1, \dots, \mathbf{x}_n; t) = G_1(\mathbf{x}_1, t) \cdots G_1(\mathbf{x}_n, t), \quad (8.74)$$

when $|\mathbf{x}_i - \mathbf{x}_j| > 2v_0t$ for all $i \neq j$. This simply reflects that there are no nucleation events that affect more than one point. Consequently, correlations vanish at large enough distances.

On the other hand, when there is a pair that is sufficiently close, correlations become nontrivial. Consider the pair correlation function $G_2(\mathbf{x}_1, \mathbf{x}_2)$ for homogeneous nucleation. The integral in (8.73) is proportional to the volume enclosed by the two hyper-cones originating at \mathbf{x}_1 and \mathbf{x}_2 (Fig. 8.12). The pair correlation function $G_2(\mathbf{x}, t) \equiv G_2(\mathbf{0}, \mathbf{x})$ may be written using the one point correlation $G_1(t) \equiv G_1(\mathbf{x}, t)$ in a way that manifests whether or not correlations are nontrivial

$$G_2(\mathbf{x}, t) = [G_1(t)]^2 \exp \left[\gamma U_d v^d t^{d+1} F_d \left(\frac{|\mathbf{x}|}{2v_0t} \right) \right]. \quad (8.75)$$

The characteristic function $0 \leq F_d(z) \leq 1$ quantifies the degree of correlation in d -dimensions. The characteristic function is normalized, $F_d(0) = 1$, and it vanishes, $F_d(z) = 0$, for $z \geq 1$.

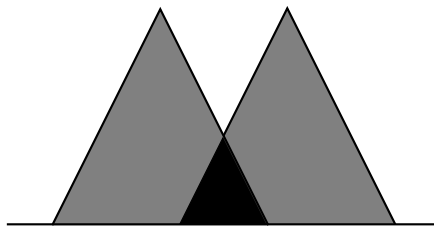


Figure 8.12: Pair correlation for homogeneous nucleation-and-growth in one-dimension. The overlap region between two spacetime triangle is highlighted.

The argument of the exponential in (8.73) equals the space-time volume of the overlap region involving two d -dimensional hyper-cones. For example, when $d = 1$, the overlap region is formed by two identical triangles of width $2v_0t$ and height t whose vertices are separated by distance $x < 2v_0t$. The overlap region is itself a triangle (figure 8.12) with width $2v_0t - x$ and height $t - x/(2v_0)$ and thus, its area is $(2v_0t - x)^2/(4v_0)$. Hence, the characteristic function is $F_1(z) = (1 - z)^2$ for $z < 1$.

Generally, the characteristic function $F_d(z)U_d = V_{\text{overlap}}(z)$ is obtained from the overlap volume $V_{\text{overlap}}(z)$ formed by two d -dimensional hyper-cones of radius 1 and height 1 whose vertices are separated by distance $2z$. Specifically,

$$F_d(z) = \begin{cases} 1 - z^2 & d = 1, \\ \frac{2}{\pi} \left[\cos^{-1} z - 2z\sqrt{1 - z^2} + z^2 \ln \frac{1 + \sqrt{1 - z^2}}{z} \right] & d = 2, \\ \frac{1}{2}(1 - z)^3(1 + z) & d = 3. \end{cases} \quad (8.76)$$

In the complementary case of instantaneous nucleation, the pair correlation can be expressed as follows

$$G_2(\mathbf{x}, t) = [G_1(t)]^2 \exp \left[\sigma V_d v^d t^d F_d \left(\frac{|\mathbf{x}|}{2v_0t} \right) \right]. \quad (8.77)$$

Now, the characteristic function $F_d(z)V_d = V_{\text{overlap}}(z)$ is obtained from the overlap volume $V_{\text{overlap}}(z)$ formed by two d -dimensional hyper-cones of radius 1 separated by distance $2z$. For instance,

$$F_d(z) = \begin{cases} 1 - z & d = 1, \\ \frac{2}{\pi} [\cos^{-1} z - z\sqrt{1 - z^2}] & d = 2, \\ \frac{1}{2}(1 - z)^2(2 + z) & d = 3. \end{cases} \quad (8.78)$$

This geometric procedure extends to higher-order correlation functions. For example, the three-point correlation function is exponential in the total volume $V_{\text{total}} = V_1 + V_2 + V_3 - (V_{12} + V_{13} + V_{23}) + 2V_{123}$ where V_i is the single-point exclusion volume, V_{ij} is the volume of the exclusion region common to two points, and V_{ijk} is the volume of the exclusion region common to three points.